A nonuniform perturbation to quantify RANS model uncertainties

By Z. Huang, A. Mishra AND G. Iaccarino

1. Motivation and objectives

There are many approaches to quantifying the uncertainties of the RANS simulations. The uncertainties of model parameters can be quantified by data-driven techniques. Cheung *et al.* (2011) employed Bayesian techniques to quantify the uncertainties for the coefficients of the Spalart-Allmaras model. Edeling *et al.* (2014) performed Bayesian estimations for the coefficients of the low-Reynolds-number $k-\epsilon$ model. The other method quantifies the uncertainties in the Reynolds stress tensor with the help of the Reynolds stress realizability (Duraisamy *et al.* 2019). Banerjee *et al.* (2007) proposed linear mapping between the eigenvalues of the Reynolds stresses and barycentric coordinates, which is easily visualized in a triangle. With the linear combination of the three corners in the barycentric triangle, the invertible relationship between the position and the eigenvalues could be obtained linearly. On the basis of the realizability and the barycentric map, Iaccarino and coworkers proposed a physics-based nonparametric method to quantify the model-form uncertainties (Emory *et al.* 2013; Gorlé & Iaccarino 2013; Gorlé *et al.* 2015; Iaccarino *et al.* 2017; Thompson *et al.* 2019). In this framework (Emory *et al.* 2013; Gorlé & Iaccarino 2013), the model uncertainties are approximated by injecting perturbations into the eigenvalue of the modeled Reynolds stress and the turbulent kinetic energy. Furthermore, the framework has been improved by considering the orientation of the eigenvectors of Reynolds stress to deal with complex flows, e.g., flow with streamline curvature (Thompson *et al.* 2019) and flow with separations and reattachments (Iaccarino *et al.* 2017). In these flows, the linear eddy viscosity hypothesis is known to be invalid since it assumes that the Reynolds stress has the same eigenvectors as the mean rate of strain. Therefore, considerable successful engineering applications have been achieved using the physics-based approaches (Emory *et al.* 2013; Gorlé & Iaccarino 2013; Gorlé *et al.* 2015; Iaccarino *et al.* 2017; Thompson *et al.* 2019).

For these approaches, all the eigenvalues of the modeled Reynolds stress are pushed to the corners uniformly in the barycentric triangle, whose corners are 1 component (1C) point with eigenvalue $\lambda_{1c} = [2/3, -1/3, -1/3]$, 2 component (2C) point with eigenvalue $\lambda_{2c} = [1/6, 1/6, -1/3]$, and 3 component (3C) point with eigenvalue $\lambda_{3c} = [0, 0, 0]$. Naively, different eigenvalues or different locations in the barycentric map have different difficulties in terms of being pushed to the same target position in the barycentric map. For example, the eigenvalues near the 3C corner related to nearly isotropic turbulence can easily be pushed to the 3C corner, whereas it would be difficult to push the eigenvalues to the 1C or 2C corner to achieve converged numerical simulations. Therefore, to obtain reliable converged simulations, certain uniform coefficients smaller than unity, like Δ_B or under-relaxation factor, are chosen to quantify the model uncertainties (Emory *et al.* 2013; Gorlé & Iaccarino 2013; Gorlé *et al.* 2015; Iaccarino *et al.* 2017; Thompson *et al.* 2019).

On the basis of an analysis of the framework of eigenvalue and eigenspace perturba-

tions, alternatively, in this study, we propose a nonuniform approach to quantify the model uncertainties and compare the simulation with the previous methods. The key idea of present method is to perturb the points with different distances instead of pushing all the points to the corners uniformly. The numerical simulations show that the perturbation simulations achieve the same well convergence as the baseline simulation; additionally, we can quantify the model uncertainties without any user-chosen coefficient.

2. Mathematical formulations

The framework of eigenvalue and eigenspace perturbations shows great practical potential in engineering applications. We introduce the basic knowledge and review the methods as follows. For the turbulence anisotropy tensor based on the eddy viscosity hypothesis,

$$b_{ij} = \frac{R_{ij}}{2k} - \frac{1}{3}\delta_{ij} = -\frac{\nu_t S_{ij}}{k}, \tag{2.1}$$

where ν_t is the turbulence eddy viscosity and S_{ij} is the mean rate of strain. Performing the eigenvalue decomposition,

$$b_{ij} = v_{in}\Lambda_{nl}v_{jl}, \tag{2.2}$$

where v_{in} is the matrix composed of eigenvectors of b_{ij} and Λ_{nl} is the diagonal matrix of eigenvalues. By injecting the perturbation into the eigenvalue directly to the corner with certain distance Δ_B, the perturbed eigenvalue is obtained

$$\Lambda^{\star\prime}_{ii} = \Lambda_{ii} + \Delta_B(\Lambda^c - \Lambda_{ii}), \tag{2.3}$$

where Λ^c is the target eigenvalue in the barycentric triangle. Then, the eigenvectors are perturbed to get the perturbed anisotropy tensor

$$b^\star_{ij} = v^\star_{in}\Lambda^\star_{nl}v^\star_{jl}. \tag{2.4}$$

Hence, the perturbed Reynolds stress is

$$R^\star_{ij} = 2kb^\star_{ij} + \frac{2}{3}k\delta_{ij}. \tag{2.5}$$

In most of the previous studies that include both eigenvalue and eigenspace perturbations (Emory *et al.* 2013; Gorlé & Iaccarino 2013; Iaccarino *et al.* 2017), the eigenvalues Λ^c locate at the triangle corners in the barycentric map. However, it should be noted that the uniform Δ_B or the under-relaxation factor β smaller than 1 is usually employed in order to achieve well-converged numerical simulations (Gorlé & Iaccarino 2013; Iaccarino *et al.* 2017). That is, the perturbed eigenvalues could not reach the eigenvalues located at the barycentric triangle corners related to the three extreme cases. Moreover, the perturbed Reynolds stresses would be very close to the modeled Reynolds stresses if Δ_B or β is very small. Therefore, there is a trade-off between the magnitude of perturbation and the reliable converged simulations, which incurs many extra efforts and simulations. In the following subsections, we analyze the eigenvalue and eigenspace perturbations in view of the production term in the turbulent kinetic energy equation, for which it is very helpful to propose the nonuniform perturbation method.

2.1. *Eigenvalue perturbation with* Δ_B

Without loss of generality, if we consider two-dimensional flows, the eigenvalues of b_{ij} are $\vec{a}$, i.e., $[-a, 0, a]$ where $a \geq 0$, and the three eigenvectors are $\vec{v}_1$, $\vec{v}_2$ and $\vec{v}_3$, respectively.

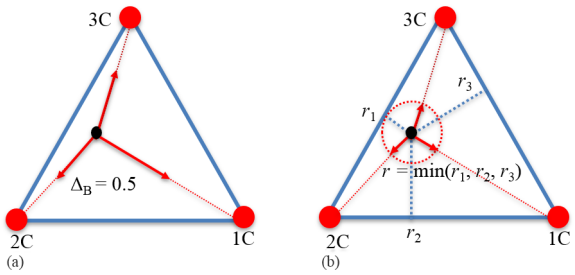

FIGURE 1. Schematic of a perturbation method with (a) constant Δ_B compared with (b) the nonuniform parameter r.

According to Eq. (2.1), S_{ij} has the eigenvalues of $-k/\nu_t\vec{a}$ and the same eigenvectors as those of b_{ij}. If we perturb the eigenvalues directly to the corners with certain uniform distance Δ_B, then the perturbed eigenvalue $\vec{\lambda}^\star$ can be written as

$$\vec{\lambda}^\star = \vec{a} + \Delta_B(\vec{\lambda}^c - \vec{a}), \tag{2.6}$$

where $\vec{\lambda}^c$ is the eigenvalue at the corner in the barycentric map. If we consider the 1C case with the eigenvalues $\vec{\lambda}^c = [-1/3, -1/3, 2/3]$, then

$$\vec{\lambda}^\star = [-a, 0, a] + \Delta_B([-1/3, -1/3, 2/3] - [-a, 0, a]). \tag{2.7}$$

For the eigenvalue perturbation, the production $\vec{a} \cdot \vec{\lambda}^\star = 2a^2 + \Delta_B(a - 2a^2)$. If the first and third eigenvectors are permuted, the minimal production is obtained $\vec{a} \cdot \vec{\lambda}^\star = -2a^2 - \Delta_B(a - 2a^2)$. As we know, the production term in the turbulent kinetic energy equation is

$$-R_{ij} * S_{ij} = -(2kb_{ij} + \frac{2}{3}k\delta_{ij}) * S_{ij}. \tag{2.8}$$

Therefore, if only the turbulence anisotropy is perturbed, then the production is determined by $-b^\star_{ij} * S_{ij}$.

In summary,

$$-b^\star_{ij} * S_{ij} = b^\star_{ij} * b_{ij}(k/\nu_t) = (k/\nu_t) \begin{cases} 2a^2(1-\Delta_B) + a\Delta_B & \text{1C} \\ -2a^2(1-\Delta_B) - a\Delta_B & \text{1C minimal} \\ 2a^2(1-\Delta_B) + a/2\Delta_B & \text{2C} \\ -2a^2(1-\Delta_B) - a/2\Delta_B & \text{2C minimal} \\ 2a^2(1-\Delta_B) & \text{3C} \\ -2a^2(1-\Delta_B) & \text{3C minimal .} \end{cases} \tag{2.9}$$

Based on the framework of the uniform eigenvalue perturbation using Δ_B, if the first and third eigenvectors are permuted directly, the negative production would be obtained. It is not surprising that the perturbed simulations do not converge as well as the baseline simulation. Moreover, the negative production is obtained even if $\Delta_B = 0$. Therefore, there is no reason to expect a converged simulation if the eigenvectors are permuted based on the eigenvalue perturbation framework using Δ_B.

2.2. *Eigenspace perturbation with under-relaxation factor*

For the eigenspace perturbation, we obtain

$$\begin{aligned} R^{\star}_{ij} &= R_{ij} + \beta * (R^{c}_{ij} - R_{ij}) \\ &= 2k * [b_{ij} + \beta * (b^{c}_{ij} - b_{ij})] + \frac{2}{3}k\delta_{ij} \\ &= 2k * b^{ES}_{ij} + \frac{2}{3}k\delta_{ij}, \end{aligned} \tag{2.10}$$

where $b^{ES}_{ij} = b_{ij} + \beta * (b^{c}_{ij} - b_{ij})$. However, we note that the eigenspace perturbation is performed to obtain $b^{c}_{ij} = v^{c}_{in}\Lambda^{c}_{nl}v^{c}_{jl}$. Therefore,

$$b^{ES}_{ij} = (1-\beta)b_{ij} + \beta * b^{c}_{ij} = (1-\beta)v_{in}\vec{a}_{nl}v_{jl} + \beta * v^{c}_{in}\Lambda^{c}_{nl}v^{c}_{jl}. \tag{2.11}$$

For the eigenvalue perturbation of the 1C case, $\vec{\lambda}^{c} = [-1/3, -1/3, 2/3]$, the production $(1-\beta) * (a_1 * a_1 + a_2 * a_2 + a_3 * a_3) + \beta * (a_1 * \lambda_1 + a_2 * \lambda_2 + a_3 * \lambda_3) = 2a^2(1-\beta) + \beta a$ achieves the maximal value without permutation of eigenvectors; for the permutation of the first and third eigenvectors, the minimal production is $(1-\beta) * (a_1 * a_1 + a_2 * a_2 + a_3 * a_3) + \beta * (a_1 * \lambda_3 + a_2 * \lambda_2 + a_3 * \lambda_1) = 2a^2(1-\beta) - \beta a$.

In summary,

$$-b^{\star}_{ij} * S_{ij} = b^{\star}_{ij} * b_{ij}(k/\nu_t) = (k/\nu_t) \begin{cases} 2a^2(1-\beta) + \beta a & \text{1C} \\ 2a^2(1-\beta) - \beta a & \text{1C minimal} \\ 2a^2(1-\beta) + \beta a/2 & \text{2C} \\ 2a^2(1-\beta) - \beta a/2 & \text{2C minimal} \\ 2a^2(1-\beta) & \text{3C} \\ 2a^2(1-\beta) & \text{3C minimal.} \end{cases} \tag{2.12}$$

We can see that if the eigenvectors are not perturbed, the eigenvalue and eigenspace perturbations are the same. The extreme productions are obtained at 1C and 1C minimal perturbations. Interestingly, the productions are the same as the baseline simulation if $\beta = 0$, and the converged simulations are expected with sufficiently small β when the production is positive. However, the difference between the extreme values is still $2\beta a$. The numerical results (Iaccarino *et al.* 2017) show that the uniform β should be smaller than 0.1 to achieve converged simulations. Interestingly, the quantities of interests are usually bounded by the two extreme production perturbations considering the case of flow separations and reattachment.

2.3. *Nonuniform perturbation*

The above perturbations are widely employed for many engineering applications (Gorlé & Iaccarino 2013; Iaccarino *et al.* 2017). However, it might be not appropriate since all the flow points are perturbed to the same corner uniformly. For example, the isotropic flow has many eigenvalues locating near the 3C corner, which are very hard or impossible to be perturbed to the other two corners. If we analyze the framework with uniform Δ_B and further with β, the point 3C corner is assigned with the largest distance directly to other corners, while the innermost point is assigned with the largest distance directly to the 3C corner. Therefore, the uniform perturbation is not favorable for the simulation convergence. Additionally, there is no theoretical guide to determine the value of Δ_B or β before extensive simulations have been performed. In this study, an alternative perturbation method has been proposed as shown in Figure 1. First, the points of the modeled Reynolds stress in the barycentric map could be captured; then, the distances

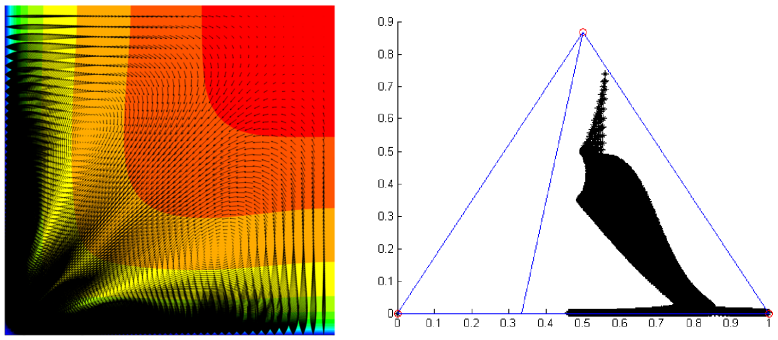

(a) (b)

FIGURE 2. Contours of streamwise velocity overlaid with (a) in-plane velocity vectors and (b) the distributions of Reynolds stress in a barycentric map for DNS data at $Re_\tau = 360$.

of each point to the three triangle lines can be calculated; finally, the shortest distance r is chosen to perturb the eigenvalue to the corners. The basic idea is that each point in the flow field is perturbed with different distance adaptively and accordingly; that is, the points near the corners are perturbed slightly and the innermost points are perturbed significantly in the barycentric map.

$$\begin{aligned} R_{ij}^H &= 2k * b_{ij}^H + \frac{2}{3}k\delta_{ij} \\ &= 2k * [v_{in}\vec{a}_{nl}v_{jl} + rv_{in}^c(\Lambda^c - \vec{a})_{nl}v_{jl}^c] + \frac{2}{3}k\delta_{ij}; \end{aligned} \tag{2.13}$$

that is, $b_{ij}^H = v_{in}\vec{a}_{nl}v_{jl} + rv_{in}^c(\Lambda^\star - \vec{a})_{nl}v_{jl}^c$. Therefore, in summary, the productions are

$$-b_{ij}^H * S_{ij} = b_{ij}^H * b_{ij}(k/\nu_t) = (k/\nu_t) \begin{cases} 2a^2(1-r) + ra & \text{1C} \\ 2a^2(1+r) - ra & \text{1C minimal} \\ 2a^2(1-r) + ra/2 & \text{2C} \\ 2a^2(1+r) - ra/2 & \text{2C minimal} \\ 2a^2(1-r) & \text{3C} \\ 2a^2(1+r) & \text{3C minimal.} \end{cases} \tag{2.14}$$

By doing this, we find that the productions are very similar to that of eigenspace perturbations. Moreover, the eigenvalues near the 3C corner are just pushed slightly since the r is very small near the corner, which might allow well convergence of the simulation. It should be noted that the eigenvalues for two-dimensional flows are constrained along the plane shear stress line in the barycentric map when the model satisfies the realizability completely. The model uncertainty quantification method is implemented and the simulations of the square duct flow and plane asymmetric diffuser are tested and compared with the previous results; additionally, the three-dimensional wind loading on the building is examined.

3. Results and discussions

3.1. *Turbulent square duct flow*

There are many valuable DNS datasets of turbulent developing flow within constant cross-section square ducts available for different Reynolds numbers (Vinuesa *et al.* 2014, 2015,

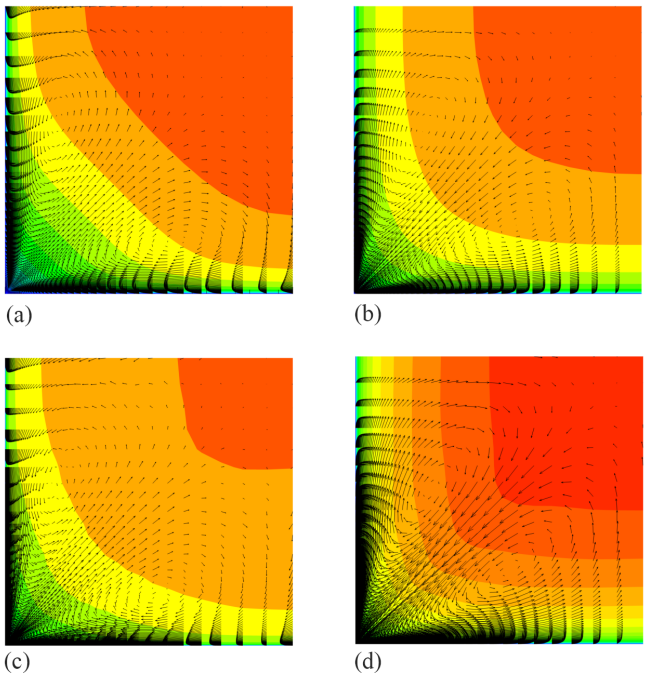

FIGURE 3. Contours of streamwise velocity overlaid with in-plane velocity vectors for (a) 1C perturbation and (b) 2C perturbation with uniform $\Delta_B = 0.5$, and (c) 1C perturbation and (d)2C perturbation with nonuniform perturbation.

2018). The computational domain of the duct has the dimension $2h \times 2h$ in wall-normal directions. The periodicity in the streamwise direction has been employed for the DNS because the developed region of the duct is of interest. However, the developing duct flow is simulated by the RANS model in a three-dimensional computational domain $200h \times h \times h$ in streamwise and wall-normal directions, and one-quarter of the duct cross-section is employed due to the symmetry. The cross-section secondary flow and Reynolds stresses in the barycentric map of the DNS data are shown in Figure 2. The turbulent square duct flow is simulated using the $k-\omega$ shear stress transport (SST) model at $Re_\tau = 360$. Although the symmetric duct flow does not have flow separation, the RANS models failed to simulate the secondary flows in the duct cross-section (Bradshaw 1987). According to the previous study (Emory *et al.* 2013), the secondary flow could be estimated by perturbing the eigenvalues in the momentum equations. However, the residuals of the baseline decrease to about 10^{-10}, while the continuity residuals are about $O(1)$ for the eigenvalue perturbations with $\Delta_B = 0.5$. The streamwise velocity and in-plane velocity vectors are shown in Figure 3. Similar to the previous study (Emory *et al.* 2013), the 1C and 2C nonuniform perturbations introduce secondary flows near the duct corners. The vortices move fluid from the corner to the core for the 1C perturbation, whereas the vortices impinge fluid from the center toward the corners for the 2C perturbation. Compared with the DNS data, where the secondary flow moves from the duct center to the corner, the 2C perturbation results in the correct flow regime. The theoretical explanation can be found in Emory *et al.* (2013) and Mishra & Iaccarino (2019).

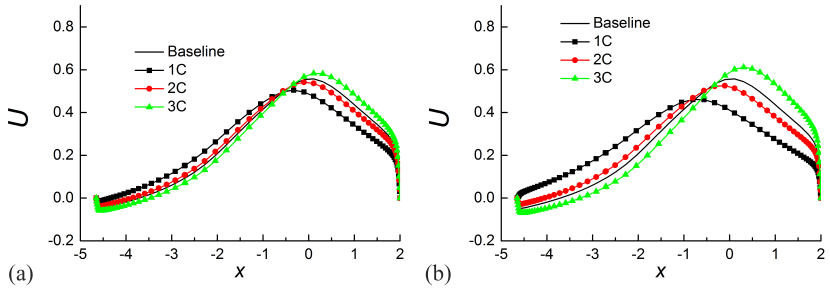

FIGURE 4. The distributions of velocity of eigenspace perturbations are compared with baseline simulations for (a) $\beta = 0.02$ and (b) $\beta = 0.04$.

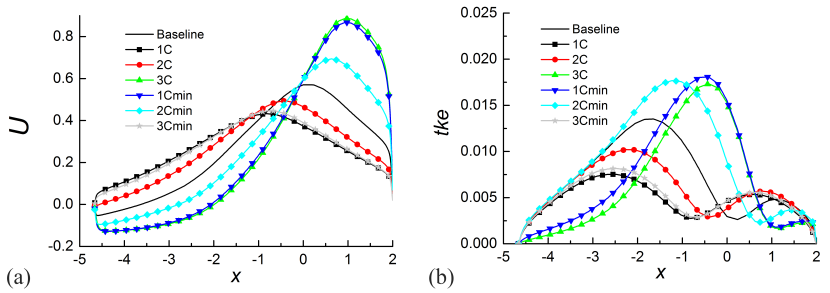

FIGURE 5. The distributions of (a) velocity and (b) turbulent kinetic energy for nonuniform perturbations.

3.2. *Plane asymmetric diffuser*

The square duct turbulent flow is developed gradually and no obvious flow separation or adverse pressure gradient occurs. In other words, there is no difficulty in simulating the square duct flow using RANS models. However, the actual flows in engineering applications are much more complicated, and the RANS models usually fail to predict the complicated flows with flow separation and reattachment, adverse pressure gradients and boundary curvatures. In such flows, the actual Reynolds stresses are misaligned with the mean rate of strain, while the eigenvalue perturbations (Emory *et al.* 2013; Gorlé & Iaccarino 2013) cannot account for the effects. Recently, the eigenspace perturbation in consideration of the possible extreme productions of Reynolds stress and mean rate of strain has been proposed by Iaccarino *et al.* (2017), which efficiently quantifies the model uncertainty for many complicated practical flows (Iaccarino *et al.* 2017; Thompson *et al.* 2019). For instance, the turbulent flow over the asymmetric diffuser involves separation from the slope wall due to an adverse pressure gradient, followed by the reattachment and redevelopment of the boundary layer in the downstream, which are the challenges for RANS models.

The two-dimensional plane asymmetric diffuser flow is simulated by the $k - \omega$ SST model. The simulations show that the well convergence could not be obtained if the under-relaxation factor β goes beyond 0.04 for the uniform eigenvalue perturbations. The simulations of eigenvalue perturbation are compared with the baseline simulation in Figure 4, and it can be seen that the uncertainty interval increases with the β. Therefore, the merits of uniform perturbations are degraded by the convergence issue and the choice of the under-relaxation factor.

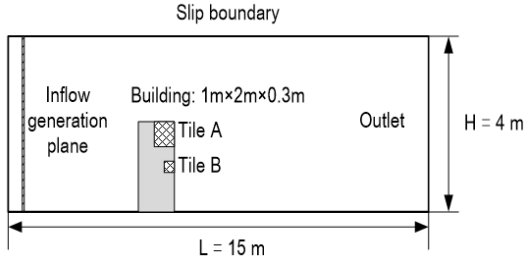

FIGURE 6. Schematic of the flow over a high-rise building in the atmospheric boundary layer.

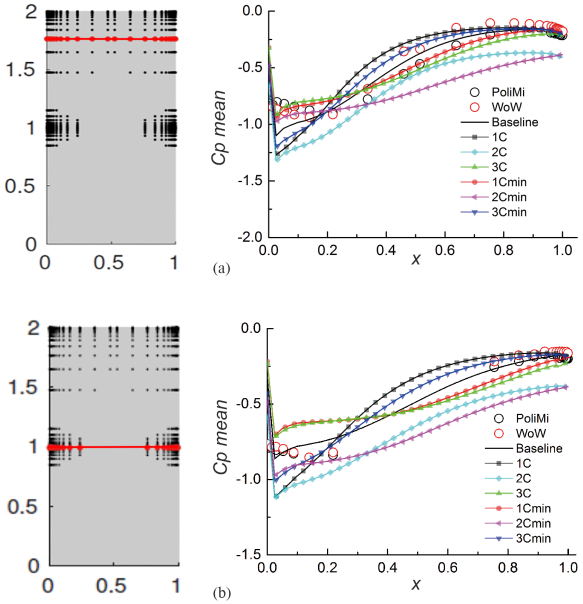

FIGURE 7. The distributions of mean pressure coefficients for nonuniform perturbations compared with experimental measurements at different building locations (a) $y = 1.76$ and (b) $y = 1$.

Although the eigenvalues are perturbed to the corners in the barycentric map, the small under-relaxation factor β limits the perturbation close to the modeled Reynolds stress. That is, the perturbed Reynolds stresses are very close to the modeled Reynolds stresses to achieve the same convergence as the baseline simulation. The extreme values or the triangle corners in the barycentric map and the largest possible uncertainties are desirable to quantify the model uncertainties. However, the small β limits the uncertainties and we need to capture the proper value of β after many trial-and-error simulations. The limitation might be attributed to the uniform perturbations near the corner, which are very difficult to push to other corners. Naively, the points near the 3C corner are difficult to push to other corners. Actually, the uniform perturbations result in a larger distance for the points near the 3C corner, compared with other points in the barycentric map. Therefore, the uniform perturbation injects large uncertainties near the 3C corner that are difficult to perturb, and the accompanied convergence issue is reasonable.

Alternatively, the Reynolds stresses that are perturbed nonuniformly might be favor-

able for convergence. Naively, the points near the corners or the lines are injected with smaller uncertainties, whereas the points near the barycentric triangle center are injected with larger uncertainties. Moreover, according to the analysis in Section 2, the difference between the extreme production terms of nonuniform perturbation is the smallest compared with the baseline simulation. These might be the reasons why the six simulations obtain the same well convergence as the baseline simulation, and the results are shown in Figure 5. Additionally, the nonuniform parameter r is determined in the simulation adaptively and we can get rid of the choice of parameters, which is another benefit of nonuniform perturbation for practical applications.

3.3. *Wind loading on a high-rise building*

In the section above, the analysis about the production is focused on two-dimensional flows. Actually, the analysis can be extended to three-dimensional flows directly. The three-dimensional flow over a high-rise building in an atmospheric boundary layer has been investigated experimentally (Lamberti *et al.* 2020) and numerically (Lamberti *et al.* 2018) due to its importance in civil engineering. We try to quantify the model uncertainties of the pressure coefficient on the building surface in this flow; the schematic of the flow is shown in Figure 6. This flow has been simulated by Re-normalisation group (RNG) $k-\epsilon$ model and the model uncertainties are quantified by the nonuniform perturbation with six simulations. The residuals converge to 10^{-5} for the perturbations, which are same for the baseline simulations. Two typical positions for the mean pressure coefficient are considered in Figure 7. Although the baseline simulation has considerable difference compared with experimental data near the leading edge, the uncertainty interval composed of the six nonuniformly perturbed simulations accounts for the discrepancy.

4. Conclusions

A new nonuniform perturbation method to quantify the RANS model uncertainty has been proposed. The eigenvalues of the modeled Reynolds stress are pushed nonuniformly in the barycentric map rather than uniformly as in previous studies (Emory *et al.* 2013; Iaccarino *et al.* 2017). The widely used $k-\omega$ SST and RNG $k-\epsilon$ models are examined in the two- and three-dimensional flows. The main advantages of the present method, compared with the previous investigations (Emory *et al.* 2013; Iaccarino *et al.* 2017), which have been demonstrated by numerical simulations, are the well convergence of simulations and the adaptively determined nonuniform perturbations. For the turbulent square duct flow, the present method results in good convergence and a secondary flow similar to the uniform eigenvalue perturbation with $\Delta_B = 0.5$ (Emory *et al.* 2013). The turbulent flow in the asymmetric diffuser, which has separation in the mean flow, has been tested. The present method achieves very good convergence, while the uniform eigenvalue perturbation (Iaccarino *et al.* 2017) requires a user-chosen under-relaxation factor. Moreover, the method is extended to simulate three-dimensional flows over bluff bodies with strong separation near the building surfaces, and the uncertainty intervals of the interested quantity account for the discrepancy between simulation and measurements. The nonuniform perturbation method should be examined by much more complicated flows in the near future.

Acknowledgments

This work was supported Los Alamos National Laboratory.

REFERENCES

Banerjee, S., Krahl, R., Durst, F. & Zenger, C. 2007 Presentation of anisotropy properties of turbulence, invariants versus eigenvalue approaches. *J. Turbul.* **1**, N32.

Bradshaw, P. 1987 Turbulent secondary flows. *Annu. Rev. Fluids Mech.* **19**, 53--74.

Cheung, S. H., Oliver, T. A., Prudencio, E. E., Prudhomme, D. & Moser, R. D. 2011 Bayesian uncertainty analysis with applications to turbulence modeling. *Reliab. Eng. Syst. Saf.* **96**, 1137--1149.

Duraisamy, K., Iaccarino, G., & Xiao, H. 2019 Turbulence modeling in the age of data. *Annu. Rev. Fluid Mech.* **51**, 357--377.

Edeling, W. N., Cinnella, P., Dwight, R. P., & Bijl, H. 2014 Bayesian estimates of parameter variability in the $k-\epsilon$ turbulence model. *J. Comput. Phys.* **258**, 73--94.

Emory, M., Larsson, J. & Iaccarino, G. 2013 Modeling of structural uncertainties in Reynolds-averaged Navier-Stokes closures. *Phys. Fluids* **25**, 110822.

Gorlé, C. & Iaccarino, G. 2013 A framework for epistemic uncertainty quantification of turbulent scalar flux models for Reynolds-averaged Navier-Stokes simulations. *Phys. Fluids* **25**, 055105.

Gorlé, C., Garcia-Sanchez C. & Iaccarino, G. 2013 Quantifying inflow and RANS turbulence model form uncertainties for wind engineering flows. *J. Wind Eng. Ind. Aerod.* **144**, 202--212.

Hoyas, S. & Jimenez, J. 2006 Scaling of the velocity fluctuations in turbulent channels up to $Re_\tau = 2003$. *Phys. Fluids* **18**, 011702.

Iaccarino, G., Mishra, A. A. & Ghili, S. 2017 Eigenspace perturbations for uncertainty estimation of single-point turbulence closures. *Phys. Rev. Fluids* **2**, 024605.

Lamberti, G., Amerio, L., Pomaranzi, G. & Gorle, C. 2020 Comparison of high resolution pressure measurements on a high-rise building in a closed and open-section wind tunnel. *J. Wind Eng. Ind. Aerod.* **204**, 104247.

Lamberti, G., Gacia-Sanchez, C., Sousa, J. & Gorle, C. 2018 Optimizing turbulent inflow conditions for large-eddy simulations of the atmospheric boundary layer. *J. Wind Eng. Ind. Aerod.* **177**, 32--44.

Mishra, A. A. & Iaccarino, G. 2017 Uncertainty estimation for Reynolds averaged Navier-Stokes predictions of high-speed aircraft nozzle jets. *AIAA J.* **55**, 11.

Mishra, A. & Iaccarino, G. 2019 Theoretical analysis of tensor perturbations for uncertainty quantification of Reynolds averaged and subgrid scale closures. *Phys. Fluids* **31**, 075101.

Thompson, R. L., Mishra, A. A., Iaccarino, G., Edeling, W. & Sampaio L. 2019 Eigenvector perturbation methodology for uncertainty quantification of turbulence models. *Phys. Rev. Fluids* **4**, 044603.

Vinuesa, R., Schlatter, P. & Nagib, H. M. 2018 Secondary flow in turbulent ducts with increasing aspect ratio. *Phys. Rev. Fluids* **3**, 054606.

Vinuesa, R., Schlatter, P. & Nagib, H. M.2015 On minimum aspect ratio for duct flow facilities and the role of side walls in generating secondary flows. *J. Turbul.* **16**, 588--606.

Vinuesa, R., Noorani, A., Lozano-Duran, A., El Khoury, G. K., Schlatter, P., Fischer, P. F. & Nagib, H. M. 2014 Aspect ratio effects in turbulent duct flows studied through direct numerical simulation. *J. Turbul.* **15**, 677--706.